

with a diminished non-radiative decay in the dissipating particle. Earlier, a one loop (first order) correction to the conventional decomposition into radiative and non-radiative parts, was proposed using a phenomenological extension, to account for the non-Markovian effects [23]. This correction aimed at moderate coupling strengths is shown here to diverge for larger coupling strengths at smaller separations. The non-Markovian process results in counter-intuitive predictions, for the case of proximal nanostructures that are either strongly absorbing or do not scatter light at all. It includes the unexpected giant enhancements of emission in surface-enhanced-Raman-spectroscopy (SERS) where a strongly absorbing rough metal structure increases the radiation exciting a molecule in the near-field, by a few orders of magnitude, but surprisingly with no apparent absorption of the photons emitted by the excited molecule. This divergence of SERS from first-principle theoretical predictions has been widening for decades, as the reported SERS enhancements grew from 10^4 to 10^{14} [24–27]. Meanwhile, anomalous enhancements of spontaneous emission near fully absorbing metal nanoparticles less than 10 nm in dimensions, that do not scatter light, have also been reported [28–32]. Oscillations in their extinction spectra along with small shifts compared to the conventional predictions due to scattering of electrons at boundaries of these small particles have been known, but these marginal dissipative effects on the permittivity do not explain the above anomalous enhancements of radiative decay [33–39]. We note that the low rates of dissipation in these small nanoparticles result in stronger coupling strengths even at large relative separations, and it necessitates the non-Markovian treatment of radiative decay suggested in this work.

The difficulty in the non-Markovian evaluations is the non-locality of the interactions. Continuing from the path based description in the above paragraphs, we use a single two-level emitter and $n - 1$ spatially distributed two-level systems to represent the proximal nanoparticle. A superposition of paths based on this distributed interacting system is an explicit description of the non-local process, both in time as well as in space. An initial state of the excited system can be described by the n interacting subsystems as

$$\psi = \{c_1 |\hat{e}_1\rangle + c_2 |\hat{e}_2\rangle + \dots c_n |\hat{e}_n\rangle\} \quad (1)$$

where $c_j^* c_j$ represents the unknown probability of excitation of the two-level system j . Here \hat{e}_j represents the canonical basis vectors in n dimensions, and $\sum_j c_j^* c_j = 1$ for a known initial state. Using these individual two-level systems as the basis for representing the collective system more concisely, $\psi = [c_1, c_2, \dots c_n]$, where the emitter is given the index 1. Radiative decay of an initial state is given by the superposition of the radiative decays of the basis states $|\hat{e}_j\rangle$.

The next section on weak coupling of the emitter with the nanoparticle determines a single initial state for this emitter-particle system, analogous to the conventional

approaches. The later section on stronger couplings and non-Markovian interactions, presents a method to build a density matrix representing the mixture of initial states of the emitter-particle system with a non-local excitation. A further orthogonalization of the initial states into pure states allows a weighted sum over the superpositions in each pure state.

I. WEAK COUPLING WITH THE NANOPARTICLE

In the regime of weak coupling, the initial state of the excited coupled system is given by

$$\psi = [\psi^e, \psi^p] \quad (2)$$

where the initial state of the particle, ψ^p , is determined using the nature of its excitation due to the given initial state of the emitter, ψ^e , under the Markovian approximation.

Without any significant loss of accuracy, the initial state of the excited particle can also be constructed in the form of n polarizable point dipoles using a balance of forces. The weak coupling with vacuum allows an evaluation of the interactions using classical fields in the dipole approximation [40–42]. The absolute values of self-energy of these representative oscillators provides the probability of excitation of the mutually interacting two-level systems. It is implicit that each two-level system has a transition energy of $\hbar\omega_0$. Given the polarization of the dipole emitter, we balance the forces at each dipole using

$$-\frac{1}{\alpha_j} \mathbf{P}_j + \sum_{k=2, k \neq j}^n \mathbf{G}(\mathbf{r}_j, \mathbf{r}_k) \mathbf{P}_k = \mathbf{E}_{\text{inc.}} = \mathbf{G}(\mathbf{r}_j, \mathbf{r}_1) \mathbf{P}_1 \quad (3)$$

where the polarizability α_j of a spherical grain in the particle can be determined from its size and the dispersive permittivity of the material, using the Clausius-Mosotti relation [43] and its extensions to include the lattice dispersion [44]. The maximum size of the grain is determined by the wavelength of emission and material properties of the nanoparticle, and the number of such polarizable oscillators n arranged in a hexagonal close packed form can be increased to meet the error tolerance allowed in the solution of the system of linear equations [44]. $\mathbf{E}_{\text{inc.}}$ is the field incident on the dipole grains due to the emitter. Solving the above coupled system of equations gives us the polarization \mathbf{P}_j for $j = 2, 3 \dots n$ representing the particle. The required Green dyad \mathbf{G} are evaluated for a given frequency ω , and is defined in the appendix. The solutions can be weighted and integrated with a line-shape around the resonance frequency of the emitter, ω_0 , if required.

After solving the above, the required Markovian superposition of paths A and A' in Figure 1 is obtained using the sum of electric fields at points \mathbf{r} due to all oscillators j including the emitter, and the total decay rate due

to the particle is evaluated by the imaginary part of the self-interaction of the emitting dipole.

$$\Gamma^r = \frac{\epsilon_0}{2\hbar} \oint \mathbf{E}(\mathbf{r})^2 d\mathbf{r} = \frac{\epsilon_0}{2\hbar} \oint \left\{ \sum_{j=1}^n \mathbf{G}(\mathbf{r}, \mathbf{r}_j) \mathbf{P}_j \right\}^2 d\mathbf{r} \quad (4)$$

$$\Gamma^{\text{total}} = \frac{4\pi q^2 \omega}{mc^2} \cdot \text{Im} \left\{ \sum_{j=2}^n \mathbf{P}_1 \mathbf{G}(\mathbf{r}_1, \mathbf{r}_j) \mathbf{P}_j \right\} + \Gamma_0 \quad (5)$$

$$= \frac{4\pi q^2 \omega}{mc^2} \cdot \text{Im} \left\{ \mathbf{P}_1 [\hat{G}_{1p} \hat{G}_{pp}^{-1} \hat{G}_{p1}] \mathbf{P}_1 \right\} + \Gamma_0 \quad (6)$$

where the values of charge q and mass m represent an electron. The explicit solution of the coupled system of equations (3) containing all the 3×3 dyads \mathbf{G} , can be rearranged concisely in the form of matrices \hat{G} where the subscripts p refer to the interaction of the elements of the particle, and 1 represents the emitter respectively [45]; see appendix for the full description. This gives us the decay rate in a form where the self-interaction due to the particle explicitly appears as a tensor in the square brackets of the above equation. The non-radiative decay rate $\Gamma^{nr} = \Gamma^{\text{total}} - \Gamma^r$.

Since this solution from equation (3) uses the coupling of $n - 1$ oscillators only in the nanoparticle, it can be always rewritten as a weighted sum of the $n - 1$ orthogonal modes of the particle if required. For particles of regular shapes like spheres, a more compact set of orthogonal modes can also be analytically constructed using the vector harmonics of the Helmholtz equation. In the weak-coupling regime, the n oscillators and the analytical vector harmonics provide identical results. But an analytical decomposition into orthogonal modes of the emitter-particle *system* is not tractable for retarded interactions, and the possible quasi-static solutions become inaccurate for stronger couplings. Whereas this description using a large set of n oscillators allows us to numerically construct the eigenstates for the coupled system even with retarded interactions, and this becomes essential in the next section. Higher the refractive index and size of the particle, larger is the number of optical paths (states) in the particle, and so is the number of orthogonal modes or the number of oscillators n , required in the summation. A nanoparticle can also produce a large density of paths when a mode is resonant. Note that this weak-coupling approximation does not include the loop that returns the photon to the emitter as shown in Figure 1. This possible re-absorption of the photon renders the initial state of system as a mixture.

II. MODERATE AND STRONG COUPLINGS WITH THE NANOPARTICLE

Proceeding from the previous section on the Markovian approximation for a weak coupling, we introduce two significant refinements to include effects of the non-Markovian interaction on the radiative decay from the

system. The former converges to the latter when separations between the emitter and the dissipating nanoparticle increase, and when the size of the particle is sufficiently large. Firstly, we construct a mixture of initial states to represent the coupled system where the photon can also be re-absorbed by the emitter. Secondly, to obtain the superposition of radiative decays over all the oscillators in an initial state and also the ensemble of initial states, we decompose this mixture into a set of orthogonal pure states.

The solution of the coupled classical system using a balance of forces, in equation (3), is used here to further construct a non-local system that shares a photon [46, 47]. Solutions \mathbf{P}_j of the n oscillators and their self energy components now represent a single photon. The off-diagonal and diagonal entries of the self energy matrix normalized by Planck's constant are given by [48]:

$$\Sigma_{jk} = \frac{\Delta E_{jk}}{\hbar} - i \frac{\Gamma_{jk}}{2} = \frac{4\pi q^2 \omega}{mc^2} \cdot \mathbf{P}_j \cdot \mathbf{G}(\mathbf{r}_j, \mathbf{r}_k) \cdot \mathbf{P}_k \quad (7)$$

$$\Sigma_{jj} = \Omega_{jj} - i \frac{4\pi q^2 \omega}{mc^2} \cdot \text{Im} \left\{ \frac{\mathbf{P}_j \cdot \mathbf{P}_j}{\alpha_j} \right\} \quad (8)$$

Ω_{jj} determines the strength of coupling of the isolated oscillators with vacuum, and the conclusions presented here are agnostic to it for weak vacuum-coupling; see [49] for more details. The real parts of the above symmetric matrix provide the rates of exchange of the photon from the dipole j to another dipole k . In the rotating wave approximation valid here as $|\Delta E_{jk}| \ll \hbar\omega_0$, the Rabi frequencies are given by the absolute value of shifts in the energy ($\Omega_{jk} = |\Delta E_{jk}|/\hbar$). The imaginary parts Γ_{jk} represent the rates of decay of the photon from dipole j due to the other dipole k , and the diagonal entries represents the self-interaction of the excited oscillators due to vacuum. The n collective modes (eigenstates) of the excited system provide us a complete set of initial states, ψ^i , and corresponding sets of phases and amplitudes of these oscillators. The mixture of these collective eigenstates that are not necessarily orthogonal, determines the Hermitian density matrix ρ of the system.

$$\Sigma |\psi^i\rangle = \lambda_i |\psi^i\rangle \quad (9)$$

$$\rho = \frac{1}{\sum_{i=1}^n |\lambda_i|} \sum_{i=1}^n |\lambda_i| |\psi^i\rangle \langle \psi^i| \quad (10)$$

The self-interaction of an initial state in the form of its eigenvalue $|\lambda|$ provides its relative weight in the mixture. As the decay rate and Rabi frequency are given by the corresponding imaginary and real parts of λ , $|\lambda|$ as well represents the relative probability for a configuration of paths given by one of the n initial states. Recall the quantum superposition required over all paths as described in the introduction (Figure 1), which is now represented using a density matrix for the initial states. The ensemble averaged total decay rate and the expected Rabi frequency of oscillation are given by, $\Gamma^{\text{total}} = -2\text{Im}\{\text{tr}(\Sigma)\}$

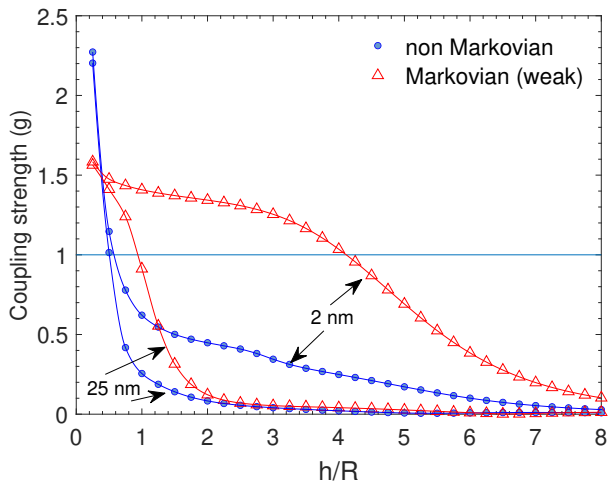


FIG. 2. Coupling strength $g = \Omega/\Gamma$ varying with the separation of the emitter h from the surface of gold particles of radii $R = 2$ nm and $R = 25$ nm in a medium of refractive index 1.5; $\hbar\omega_0 = 2.21$ eV. Here, $\Gamma = \Gamma^{\text{total}} - \Gamma_0^{nr}$. Initial state of emitter is X or Y polarized. Ω can be notably different for the two models [49].

and $\langle \Omega \rangle = \sum_{i=1}^n |\text{Re}\{\lambda_i\}|$. The predictions of Rabi frequencies can be notably different in the non-Markovian model, as shown by the coupling strengths in Figure 2.

We decompose the mixture of initial states into a set of orthogonal pure states, and this allows us to sum over the superpositions of the radiative decay from the oscillators in each orthogonal state, to evaluate Γ^r alone. Solving Hermitian eigenvalue problems $\rho|\phi^i\rangle = p_i|\phi^i\rangle$, we have probabilities p_i and the pure states ϕ^i in the mixture. The amplitude and the relative phase of an oscillator in the pure state ϕ^i , is used with the normalized polarization set by the solution of the coupled system in equation (3). The polarization of dipoles j for state ϕ^i are given by the corresponding entries of the vector:

$$\mathbf{P}_j^i = \phi_j^i \mathbf{P}_j / \|\mathbf{P}_j\| \quad (11)$$

The radiative decay rates Γ_i^r of a pure state ϕ^i is evaluated using the polarization given by the above equation and the conventional integral for the superposition of the radiated field from all oscillators j as in equation (4). The expected radiative decay rate of the system is given by $\Gamma^r = \sum_{i=1}^n p_i \Gamma_i^r$. The decay rates and Rabi frequencies of the initial states can also be used to simulate the exponentially damped oscillatory dynamics of decay, if required [50]. They result in multi-exponential decays in ensembles [18, 20], but our interest here is limited only to the efficiency of emission and time-averaged quantities.

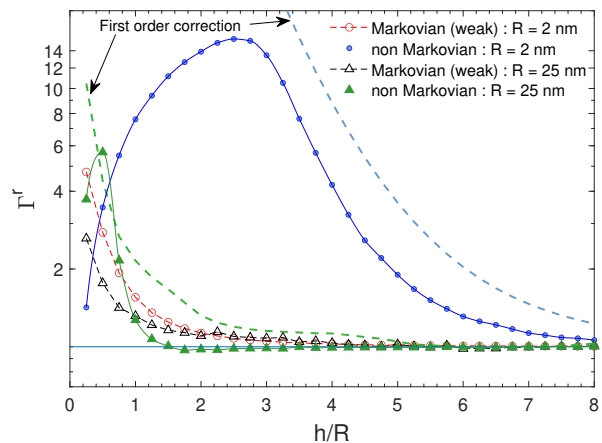


FIG. 3. Radiative decay rates Γ^r normalized by free-space decay rates Γ_0^r for emission energy $\hbar\omega_0 = 2.21$ eV at varying separations h from gold nanospheres. Initial state of emitter is X or Y polarized. The first order correction of the Markovian model [23] is given by the dashed lines. This correction for effective values was given by $\Gamma_{eff}^r = \Gamma^r + e^{-1/g} \cdot \Gamma_1^{nr}$, where subscript ‘1’ represents the dipole mode.

III. RESULTS AND DISCUSSION

In this section, we compare the results of the Markovian approximation described in section I, and the non-Markovian evaluations described in section II, for gold nanospheres of various sizes and separations from the emitter. The plots of the radiative decay in Figure 3 show an unconventional large peak for the 2 nm radii fully absorbing metal particles even at large relative separations. The earlier proposed first order correction of the Markovian evaluations suited for weak coupling, captures the large increase of radiative decays, but it diverges for smaller separations and larger coupling strengths.

Similarly, the quantum efficiencies shown in Figure 4 for X or Y polarized initial state of emitter contrast the predictions of the Markovian model with its large enhancements for the smaller fully absorbing particles in a medium of index 1.5. The plasmon resonance of the gold nanoparticles in this medium is strong at this energy of 2.21 eV, and the corresponding values for Z-polarization in Figure 5 show suppressed quenching in these cases. The movement of the peak efficiencies towards the smaller separations, and the possible enhancement due to smaller particles, are significant for unraveling the mechanism of SERS. The rough metal surface and its smaller features while enhancing the incident radiation in its near-field, are also shown here to enhance the emission from the molecules at such separations less than 10 nm. Further, the larger Γ^r predicted in the non-Markovian model can play a significant role in the SERS gains, due to the repeated excitations possible [23].

The Markovian models of coupling considered only the uncertainty of the path of the photon from the emit-

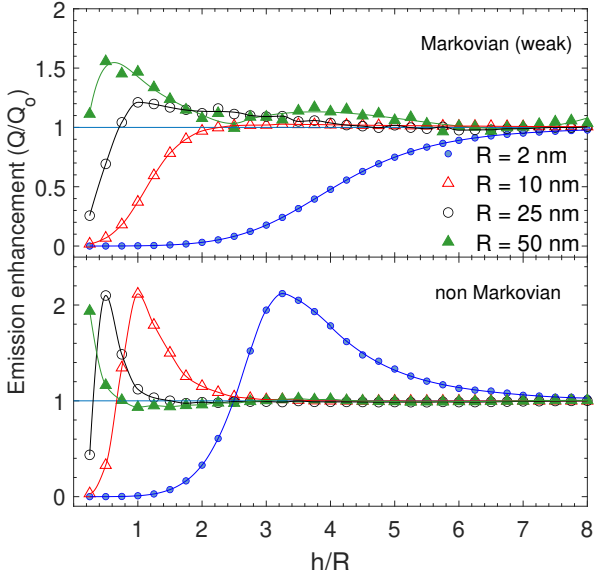


FIG. 4. Normalized quantum efficiencies for an X or Y polarized initial state of emitter show enhancement of $Q=\Gamma^r/\Gamma^{total}$ for even the smaller 2 nm gold nanoparticles, in the case of the non-Markovian model. $Q_0=1/3$ was assumed; the enhancements have an inverse relationship with Q_0 .

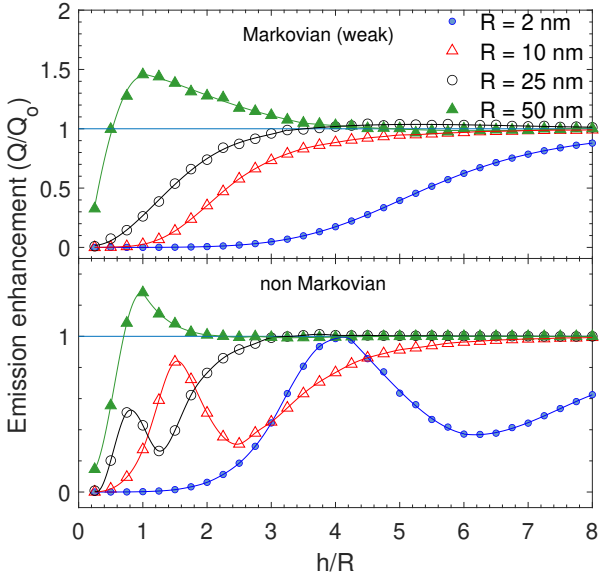


FIG. 5. Normalized quantum efficiencies for a Z-polarized initial state of emitter show suppressed quenching for the smaller gold nanoparticle, in the case of the non-Markovian model. $Q_0=1/3$ was assumed, and the enhancements have an inverse relationship with Q_0 .

ter, and the corresponding interference. In the case of proximal strongly absorbing structures, or fully absorbing (non-scattering) nanostructures, the large effect of the possible re-absorption of photons from the excited nanostructure by the proximal emitter at ground-state, represented by a non-Markovian loop in Figure 1, has to

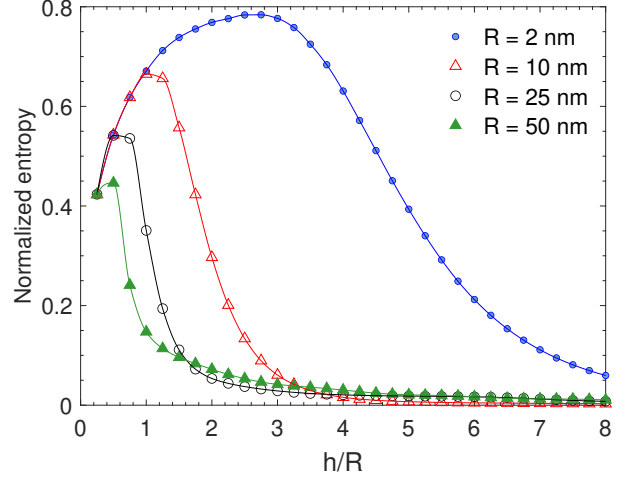


FIG. 6. The normalized von Neumann entropy of the mixture, $-\frac{1}{\log n} \sum_1^n p_i \log p_i$, varying with relative separations for gold particles of different radii R . Initial state of emitter was X or Y polarized and number of oscillators n is 1419.

be accounted by a mixture of initial states of the system; see Figure 6 for entropy of the mixtures. From a classical perspective, one may relate the origin of this effect to the evanescent fields [51] of the excited dissipating nanostructure, coupling back to the emitter at ground-state.

ACKNOWLEDGMENTS

M.V. thanks Girish S. Agarwal for illuminating discussions of the literature on self-interactions. K.J. and M.V. thank the department of Computational & Data Sciences, Indian Institute of Science for its generous support.

Appendix A: Green Dyads

The required dyads \mathbf{G} for interaction among the point-dipoles, are solutions for a point source in a homogeneous background:

$$\nabla \times \nabla \times \mathbf{G}(\mathbf{r}, \mathbf{r}_j; \omega) - k^2 \mathbf{G}(\mathbf{r}, \mathbf{r}_j; \omega) = \mathbf{I} \delta(\mathbf{r} - \mathbf{r}_j). \quad (\text{A1})$$

giving us

$$\mathbf{G}(\mathbf{r}_i, \mathbf{r}_j; \omega) = (\mathbf{I} + \frac{\nabla \nabla}{k^2}) g(\|\mathbf{r}_i - \mathbf{r}_j\|) \quad (\text{A2})$$

where $g(r) = \frac{e^{ikr}}{4\pi r}$. \mathbf{I} is a unit dyad and the wave number $k = \sqrt{\epsilon} \frac{\omega}{c}$, and $\delta(\mathbf{r} - \mathbf{r}_j)$ represents the point source at \mathbf{r}_j . The global matrix of Green tensors \hat{G} can be written in terms of the 3×3 dyads \mathbf{G} as

$$\hat{G}_{pp}(3j \rightarrow 3j + 2, 3k \rightarrow 3k + 2) = \mathbf{G}(\mathbf{r}_j, \mathbf{r}_k; \omega) \quad (\text{A3})$$

$$\hat{G}_{1p}(1 \rightarrow 3, 3j \rightarrow 3j + 2) = \mathbf{G}(\mathbf{r}_1, \mathbf{r}_j; \omega) \quad (\text{A4})$$

and $\hat{G}_{1p}^T = \hat{G}_{p1}$, where the indices $j, k = 1, 2, 3, \dots, n-1$ represent oscillators in the particle. Thus, \hat{G}_{1p} is of size $3 \times 3(n-1)$ and \hat{G}_{pp} is of size $3(n-1) \times 3(n-1)$.

-
- [1] J. Bellessa, C. Bonnand, J. C. Plenet, and J. Mugnier, *Phys. Rev. Lett.* **93**, 036404 (2004).
- [2] G. Zengin, M. Wersäll, T. J. Nilsson, S. Antosiewicz, M. Kall, and T. Shegai, *Phys. Rev. Lett.* **114**, 157401 (2015).
- [3] A. E. Schlather, N. Large, A. S. Urban, P. Nordlander, and N. J. Halas, *Nano Lett.* **13**, 3281 (2013).
- [4] N. Vats, S. John, and K. Busch, *Phys. Rev. A* **65**, 043808 (2002).
- [5] D. E. Chang, A. S. Sørensen, P. R. Hemmer, and M. D. Lukin, *Phys. Rev. B* **76**, 035420 (2007).
- [6] A. Trügler and U. Hohenester, *Phys. Rev. B* **77**, 115403 (2008).
- [7] C. Van Vlack, P. T. Kristensen, and S. Hughes, *Phys. Rev. B* **85**, 075303 (2012).
- [8] A. Delga, J. Feist, J. Bravo-Abad, and F. J. Garcia-Vidal, *Phys. Rev. Lett.* **112**, 253601 (2014).
- [9] M. Pelton, S. D. Storm, and H. Leng, *Nanoscale* **11**, 14540 (2019).
- [10] M. Macovei, J. Evers, G.-x. Li, and C. H. Keitel, *Phys. Rev. Lett.* **98**, 043602 (2007).
- [11] V. Shatokhin, C. Müller, and A. Buchleitner, *Phys. Rev. Lett.* **94**, 043603 (2005).
- [12] A. Safari, R. Fickler, E. Giese, O. S. Magaña-Loaiza, R. W. Boyd, and I. De Leon, *Phys. Rev. Lett.* **122**, 133601 (2019).
- [13] S. Evangelou, V. Yannopoulos, and E. Paspalakis, *Phys. Rev. A* **83**, 055805 (2011).
- [14] R. Bardhan, N. K. Grady, J. R. Cole, A. Joshi, and N. J. Halas, *ACS Nano* **3**, 744 (2009).
- [15] D. Kim, H. Yokota, T. Taniguchi, and M. Nakayama, *J. Appl. Phys.* **114**, 154307 (2013).
- [16] H. C. Park, Isaeni, S. Gong, and Y.-H. Cho, *Small* **13**, 1701805 (2017).
- [17] M. Venkatapathi, *J. Quant. Spectros. Radiat. Transfer* **113**, 1705 (2012).
- [18] K. H. Madsen, S. Ates, T. Lund-Hansen, A. Löffler, S. Reitzenstein, A. Forchel, and P. Lodahl, *Phys. Rev. Lett.* **106**, 233601 (2011).
- [19] D. M. Kennes, O. Kashuba, M. Pletyukhov, H. Schoeller, and V. Meden, *Phys. Rev. Lett.* **110**, 100405 (2013).
- [20] G. Agarwal, *Quantum Optics* (Cambridge University Press, 2013), ISBN 9781107006409.
- [21] A. Gonzalez-Tudela, F. J. Rodríguez, L. Quiroga, and C. Tejedor, *Phys. Rev. B* **82**, 115334 (2010).
- [22] C.-J. Yang and J.-H. An, *Phys. Rev. B* **95**, 161408 (2017).
- [23] K. Jain and M. Venkatapathi, *Phys. Rev. Appl.* **11**, 054002 (2019).
- [24] G. C. Schatz, M. A. Young, and R. P. Van Duyne, in *Surface-enhanced Raman scattering* (Springer, 2006), pp. 19–45.
- [25] M. Moskovits, *Phys. Chem. Chem. Phys.* **15**, 5301 (2013).
- [26] K. Kneipp, *J. Phys. Chem. C* **120**, 21076 (2016).
- [27] S. Heeg, N. S. Mueller, S. Wasserroth, P. Kusch, and S. Reich, *J. Raman Spectrosc.* **52**, 310 (2021).
- [28] M. Haridas and J. K. Basu, *Nanotechnol.* **21**, 415202 (2010).
- [29] M. Haridas, J. K. Basu, D. J. Gosztola, and G. P. Wiederrecht, *Appl. Phys. Lett.* **97**, 189 (2010).
- [30] K. A. Kang, J. Wang, J. B. Jasinski, and S. Achilefu, *J. Nanobiotechnol.* **9**, 16 (2011).
- [31] M. Haridas, J. K. Basu, A. K. Tiwari, and M. Venkatapathi, *J. Appl. Phys.* **114**, 064305 (2013).
- [32] R. Dutta, K. Jain, M. Venkatapathi, and J. K. Basu, *Phys. Rev. B* **100**, 155413 (2019).
- [33] A. Kawabata and R. Kubo, *Journal of the Physical Society of Japan* **21**, 1765 (1966).
- [34] F. Fujimoto and K.-i. Komaki, *Journal of the Physical Society of Japan* **25**, 1679 (1968).
- [35] R. Ruppin, *The Journal of Chemical Physics* **76**, 1681 (1982).
- [36] G. S. Agarwal and S. V. O’Neil, *Phys. Rev. B* **28**, 487 (1983).
- [37] V. M. Agranovich and V. Ginzburg, *Crystal Optics with Spatial Dispersion, and Excitons* (Springer, 1984).
- [38] U. Kreibig and M. Vollmer, *Optical Properties of Metal Clusters* (Springer, 1995).
- [39] J. A. Scholl, A. L. Koh, and J. A. Dionne, *Nature* **483**, 421 (2012).
- [40] R. Feynman and F. Vernon Jr., *Annals of Physics* **24**, 118 (1963).
- [41] J. Tignon, P. Voisin, C. Delalande, M. Voos, R. Houdré, U. Oesterle, and R. P. Stanley, *Phys. Rev. Lett.* **74**, 3967 (1995).
- [42] V. Debierre, T. Durt, A. Nicolet, and F. Zolla, *Phys. Lett. A* **379**, 2577 (2015).
- [43] E. M. Purcell and C. R. Pennypacker, *Astrophys. J.* **186**, 705 (1973).
- [44] B. T. Draine and P. J. Flatau, *J. Opt. Soc. Am. A* **11**, 1491 (1994).
- [45] M. Venkatapathi, *J. Opt. Soc. Am. B* **31**, 3153 (2014).
- [46] A. A. Svidzinsky, J. Chang, and M. O. Scully, *Phys. Rev. A* **81**, 053821 (2010).
- [47] R. Wiegner, J. Von Zanthier, and G. S. Agarwal, *Phys. Rev. A* **84**, 023805 (2011).
- [48] V. N. Pustovit and T. V. Shahbazyan, *Phys. Rev. B* **82**, 075429 (2010).
- [49] Supplementary material at [URL inserted by publisher] for additional information on simulated results (2021).
- [50] M. Otten, R. A. Shah, N. F. Scherer, M. Min, M. Pelton, and S. K. Gray, *Phys. Rev. B* **92**, 125432 (2015).
- [51] P. M. Adam, L. Salomon, F. de Fornel, and J. P. Goudonnet, *Phys. Rev. B* **48**, 2680 (1993).